A Section 508–conformant HTML version of this article is available at https://doi.org/10.1289/EHP4178.

Airway Hyperresponsiveness, Inflammation, and Pulmonary Emphysema in Rodent Models Designed to Mimic Exposure to Fuel Oil–Derived Volatile Organic Compounds Encountered during an Experimental Oil Spill

Óscar Amor-Carro,[1,2] Kathryn M. White,[1] Rebeca Fraga-Iriso,[1,2] Luis A. Mariñas-Pardo,[1] Laura Núñez-Naveira,[1] Beatriz Lema-Costa,[1] Marta Villarnovo,[1] Héctor Verea-Hernando,[1] and David Ramos-Barbón[1,2]

[1]Respiratory Research Unit, Complexo Hospitalario Universitario and the Instituto de Investigación Biomédica de A Coruña, A Coruña, Spain
[2]Respiratory Department, Hospital de la Santa Creu i Sant Pau and the Biomedical Research Institute (IIb Sant Pau), Barcelona, Spain

Background: Fuel oil–derived volatile organic compounds (VOCs) inhalation is associated with accidental marine spills. After the *Prestige* petroleum tanker sank off northern Spain in 2002 and the *Deepwater Horizon* oil rig catastrophe in 2009, subjects involved in environmental decontamination showed signs of ongoing or residual lung disease up to 5 y after the exposure.

Objectives: We aimed at investigating mechanisms driving persistent respiratory disease by developing an animal model of inhalational exposure to fuel oil–derived VOCs.

Methods: Female Wistar and Brown Norway (BN) rats and C57BL mice were exposed to VOCs produced from fuel oil mimicking the *Prestige* spill. Exposed animals inhaled the VOCs 2 h daily, 5 d per week, for 3 wk. Airway responsiveness to methacholine (MCh) was assessed, and bronchoalveolar lavage (BAL) and lung tissues were analyzed after the exposure and following a 2-wk washout.

Results: Consistent with data from human studies, both strains of rats that inhaled fuel oil–derived VOCs developed airway hyperresponsiveness that persisted after the washout period, in the absence of detectable inflammation in any lung compartment. Histopathology and quantitative morphology revealed the development of peripherally distributed pulmonary emphysema, which persisted after the washout period, associated with increased alveolar septal cell apoptosis, microvascular endothelial damage of the lung parenchyma, and inhibited expression of vascular endothelial growth factor (VEGF).

Discussion: In this rat model, fuel oil VOCs inhalation elicited alveolar septal cell apoptosis, likely due to DNA damage. In turn, the development of a peculiar pulmonary emphysema pattern altered lung mechanics and caused persistent noninflammatory airway hyperresponsiveness. Such findings suggest to us that humans might also respond to VOCs through physiopathological pathways different from those chiefly involved in typical cigarette smoke–driven emphysema in chronic obstructive pulmonary disease (COPD). If so, this study could form the basis for a novel disease mechanism for lasting respiratory disease following inhalational exposure to catastrophic fuel oil spills. https://doi.org/10.1289/EHP4178

Introduction

The health consequences of occupational or accidental inhalation of oil-derived volatile organic compounds (VOCs) have been studied in various settings (Hauser et al. 1995; Koh et al. 2014; Raabe et al. 1998; Singhal et al. 2007; Uzma et al. 2008; Woodin et al. 1998). Particularly, the exposure of cleanup workers and volunteers to oil spills has raised special concern and achieved extensive media coverage due to the repetitiveness of large environmental catastrophes caused by petroleum tanker and marine oil rig disasters (Jernelöv 2010; Zock et al. 2011). Studies on oil VOC exposure by cleaning personnel reported a variety of acute and short-term effects, including manifestations consistent with upper airway and whole respiratory tract irritation. Such data were collected from the *Deepwater Horizon* leak (Alexander et al. 2018; Goldstein et al. 2011) and other spills (Campbell et al. 1993, 1994; Janjua et al. 2006; Lyons et al. 1999; Meo et al. 2008, 2009; Morita et al. 1999). Asthma attacks were also reported (Eggleston 2007; Goldstein et al. 2011; Leikauf 2002; Nurmatov et al. 2013).

In 2002, the oil tanker *Prestige* split and sank approximately 200 km off the coast of Galicia in northwest Spain. As a result, over 60,000 tons of class 2B fuel oil with high aromatic hydrocarbon content were spilled in the ocean (Rodríguez-Trigo et al. 2007). Dragged by currents and tides, successive floating layers of viscous fuel spread over large surfaces, affecting more than 1,000 km of coast, mainly in Spain and also reaching Portugal and France (Zock et al. 2007). This caused one of the most massive environmental catastrophes before the *Deepwater Horizon* oil rig spill in the Gulf of Mexico in 2009. During several months following the *Prestige* spill, at least 300,000 persons, including volunteers, fishers, military, and fuel company workers, inhaled VOCs through their involvement in cleaning activities. Exposed subjects showed acute short-term symptoms including headache, dizziness, nausea, erythema, and upper airway irritation (Carrasco et al. 2006; Rodríguez-Trigo et al. 2007; Suárez et al. 2005), as well as increased DNA damage (Laffon et al. 2006). An extensive epidemiological study was subsequently conducted in which the subjects' respiratory symptoms, lung function, and markers of inflammation were analyzed. The data revealed evidence of increased upper and lower respiratory tract symptom frequency (Zock et al. 2007), airway hyperresponsiveness (Rodriguez-Trigo et al. 2006; Zock et al. 2011) with no difference in baseline spirometry (Rodríguez-Trigo et al. 2010), and higher concentrations of vascular endothelial growth factor (VEGF), basic fibroblast growth factor (bFGF), and the oxidative stress marker 8-isoprostane in exhaled breath condensate (Rodríguez-Trigo et al. 2010). Since 2 y elapsed from oil VOCs exposure to data collection, the reports suggested late respiratory system effects. The lower respiratory tract symptoms persisted in a subsequent survey at 5 y after the exposure (Zock et al. 2012). The concern over respiratory sequelae persisting after VOCs inhalation caused by an environmental spill has been recently revisited through the analysis of spirometry data from a large cohort exposed to the

Address correspondence to David Ramos-Barbón, Servei de Pneumologia, Mòdul 2-4[a] Plta, Hospital de la Santa Creu i Sant Pau, Sant Antoni Maria Claret 167, 08025 Barcelona, Spain. Telephone: +34 93 556 5970. Fax: +34 93 556 5601. Email: dramosb@santpau.cat

Supplemental Material is available online (https://doi.org/10.1289/EHP4178).

The authors declare they have no actual or potential competing financial interests.

Received 16 July 2018; Revised 24 December 2019; Accepted 2 January 2020; Published 12 February 2020.

Deepwater Horizon leak. Among the spill response and cleanup workers, the studies found a higher risk of lung function decline at 1–3 y after the disaster in those subjects directly involved in decontamination procedures or recovery of oily plants, wildlife, or dead animals, and in those highly exposed to burning oil or gas (Gam et al. 2018a, 2018b).

The data from the *Prestige* and the *Deepwater Horizon* studies suggest the presence of late, persistent pathogenic mechanisms or unresolved lung damage underlying the abnormalities observed. Such a hypothesis and the limitations of the field studies to provide an insight into the disease mechanisms involved led us to develop a rodent model of oil-derived VOC inhalation mimicking exposure to the *Prestige* spill. Data were collected at two time points: upon the termination of exposure and following a washout period, to reflect, respectively, early and late effects on pulmonary function, inflammation, and lung structure.

Methods

The study protocol and experimental procedures were approved by a Government Animal Ethics Committee (Comité Ético de Experimentación Animal of Xunta de Galicia) in compliance with European Union Directive 86/609 (https://op.europa.eu/en/publication-detail/-/publication/cc3a8ccb-5a30-4b6e-8da8-b13348caeb0c/language-en) and Royal Decree 1201/2005 of Spain (https://www.boe.es/eli/es/rd/2005/10/10/1201). Animal handling, experimental procedures, and data collection and reporting were carried out in compliance with the Animal Research: Reporting In Vivo Experiment (ARRIVE) guidelines (Kilkenny et al. 2010).

Animals

Female Wistar and Brown Norway (BN) rats and female C57BL/6 mice were purchased from Harlan Interfauna Ibérica and housed in polycarbonate cages (four to five mice or two to three rats per cage) assembled within a high-efficiency particulate air (HEPA)–filtered ventilated rack under controlled temperature (21–24°C) and humidity (40–55%), with a 12/12-h light/dark cycle and *ad libitum* access to food (Harlan Interfauna Ibérica) and water. Rats and mice were purchased with a specified 6-wk age upon delivery, and a 7-d adaptation period followed animal supply before carrying out any experimental procedures. At the time point of pulmonary function testing, the animals were 10–13 wk old, with the rats weighing 150–180 g and the mice 18–23 g. Pulmonary function testing was normalized on a per-animal weight basis recorded at the moment of anesthesia induction.

Study Design

Each set of experiments comprised a group of animals exposed to fuel oil vapors during 2-h sessions, 5 times per week, for 3 wk. Additional groups underwent the same exposure schedule and were then left unexposed, breathing HEPA-filtered air only, for a 2-wk washout period before data collection. The latter was aimed at capturing lasting effects, such as those reported from human subjects after an elapsed time following the *Prestige* fuel oil exposure (Rodríguez-Trigo et al. 2010; Zock et al. 2007, 2012). Nonexposed animals breathing HEPA-filtered air acted as control groups. The control, exposed, and exposed with postexposure washout groups are hereinafter referred to as "Control," "Exposed," and "Rested," respectively, for all figures and data tables. All experimental groups were $n = 6$, and the animals were randomly assigned to each experimental group.

Because airway responsiveness to methacholine (MCh) challenge was increased in the exposed human subjects, our starting hypothesis on the underlying pathophysiology was oriented at an immune-driven response eliciting airway inflammation. Since we had no clue *a priori* on the immunobiological pathways that might be involved, we tested the Wistar and BN rat strains, which have a constitutive immune deviation toward T helper 1 (Th1) and Th2 responses, respectively. The development of results from the rat strains and the C57/BL6 mouse brought us to limit our experiments to the C57/BL6 strain in the case of the mouse.

Fuel Oil Source and Specifications

The *Prestige* fuel oil was classified number 6 as per the American Society for Testing and Materials (ASTM, http://www.astm.org/cgi-bin/resolver.cgi?D396-19a) and number 2 as per the French National Organization for Standardization (AFNOR, https://www.boutique.afnor.org/standard/m15-011/liquid-mineral-fuels-properties-of-heavy-fuel-oil-no-2/article/727394/fa018130) (Rodríguez-Trigo et al. 2007). A heavy fuel oil blend resembling the spill released by the *Prestige* tanker was synthesized and generously provided by Repsol (Repsol Technology Center). Table S1 summarizes the fuel oil parameters.

Exposure System

The animals were exposed to fuel oil vapor inhalation using a flow-through exposure tower [Electro-Medical Measurement Systems (EMMS)]. This equipment was specially adapted for this project by EMMS engineers (Figure S1) in consultation with the British Toxicology Society. An inhalation tower designed for homogeneous gas distribution was fed a constant airflow that passed through a fuel oil–vaporizing chamber and was delivered throughout the tower to nose-only exposure ports. Setup testing showed no oxygen depletion at the exposure ports. For each 2-h exposure session, 2 mL of fuel oil was poured into a vapor generator immersed in a 60°C water bath to decrease oil viscosity and improve vapor release. The constant airflow was maintained throughout the circuit by balance-controlled positive and negative air pumps. Air pressure was slightly negative at the exposure ports to ensure that the animals were only inspiring air as demanded by spontaneous tidal respiration and were not breathing forcefully. The fuel oil–contaminated air was filtered through a series of charcoal filters and dehumidified through silica gel filters before it was released into a certified chemicals exhaust hood hosting the equipment.

Fuel Oil Volatile Organic Compound Composition

Benzene, toluene, ethylbenzene, and xylene (BTEX) contents were determined at the inhalation ports to quantitatively assess VOCs in the air inhaled by the animals. BTEX was measured using PerkinElmer thermal desorption tubes (Sigma-Aldrich) and an air sampling pump set to sample at 60.08-mL/min flow for 2 h in sequential 30-min samples that were analyzed separately. The samples were eluted by thermal desorption TurboMatrix ATD-400 (TurboMatrix; PerkinElmer) into an SGE-BPX capillary column (Grace) and analyzed by gas chromatography coupled to an ion trap gas spectrometer (Polaris Q; Thermo Finnigan). The experimental fuel oil–derived VOCs peaked at 30 min and decreased over time. Table 1 summarizes the BTEX measurements. VOCs composition comprised the BTEX compounds reported in the field measurements performed by the Spanish government research agency Consejo Superior de Investigaciones Científicas (CSIC) during the coast cleaning labors that followed the *Prestige* catastrophe (CSIC 2003, 2005). However, direct comparisons of the proportions of each BTEX compound are limited by several factors. In the CSIC field measurements, the BTEX content was analyzed as milligrams per kilogram in the transported fuel oil, the marine residues, and the coastal deposits, but not as its concentration in the ambient air where the cleaning crews were working. Also, the volatilization kinetics of

Table 1. Volatile organic compounds (VOCs) analysis at inhalation ports.

Time (min)	Benzene (ng)	Toluene (ng)	Ethylbenzene (ng)	m- + p-Xylene (ng)	o-Xylene (ng)
0–30	17.2	1,122.0	344.0	643.0	661.0
30–60	12.4	503.0	31.3	64.0	53.0
60–90	12.4	602.0	24.3	51.7	38.8
90–120	7.9	448.0	6.9	10.6	6.4
Total (ng)	49.9	2,675.0	406.5	769.3	759.2
Air concentration ($\mu g/m^3$)	6.92	371.03	56.38	106.70	105.30

Note: Benzene, toluene, ethylbenzene, and meta-, para-, ortho-xylene isomers (BTEX) gas chromatography analysis. A 2-mL fuel oil aliquot was delivered into the vaporization chamber over 2 h as for the animal exposure experiments. Air samples were collected at the inhalation ports of the exposure tower during the time intervals indicated. For each BTEX compound, the mass collected during each time interval and its total for the entire period are expressed in nanograms (ng). Whole air concentration is calculated from the total mass divided by the total sampled volume and expressed as micrograms per cubic meter ($\mu g/m^3$).

the various BTEX compounds differ, and the fuel oil reaching extensive coastal areas did not preserve full stability in its composition. Considering such limitations to correlate the BTEX air concentrations in our model with the BTEX relative masses in the field-sampled fuel oil, our data suggest a higher release of toluene by the fuel oil employed in our model. Due to the impossibility of obtaining samples of the original fuel oil as released by the *Prestige* tanker, synthesizing the experimental fuel oil for this work was considered a best feasible approach to model the environmental exposure.

Airway Hyperresponsiveness to Methacholine

To study the effects of fuel oil vapor inhalation on lung function, airway hyperresponsiveness to MCh was evaluated 3 d after the last exposure or following the 2-wk washout period. FlexiVent® equipment (SCIREQ) was employed for rodent mechanical ventilation and pulmonary function testing by forced oscillation technique using a linear first-order single-compartment model. The animals were anesthetized with 4% inhaled sevoflurane (Sevorane®; Abbott Laboratories) and subjected to tracheotomy with standardized tracheal cannulae (EMMS). Neuromuscular blockade was induced with 1 mg/kg of intraperitoneal rocuronium bromide (Organon Pharmaceuticals). Mechanical ventilation was set (mice/rats, respectively) at 250/90 breaths per minute with a tidal volume of 0.14/1.5 mL and 2/3 cmH_2O positive end-expiratory pressure (PEEP). Following baseline measurements, the animals were administered doubling doses of aerosolized MCh (Sigma-Aldrich) (Figure 1) with 25 µL of each solution delivered into an Aeroneb ultrasonic nebulizer (Aeroneb® Lab Nebuliser, Buxco Research Systems) connected to the inspiratory arm of the FlexiVent® ventilator. Following each MCh dose, pulmonary resistance (R_L) was measured every 15 s for 5 min to capture the postdose R_L peak.

Bronchoalveolar Lavage Collection and Analysis

Following pulmonary function recordings, the animals were euthanized under deep anesthesia by intravenous injection of 0.3 mL of 7.45% potassium chloride (Braun). Bronchoalveolar lavage (BAL) was immediately harvested through the tracheal tube by use of 5 mL of saline in 1-mL fractions for the mice and 25 mL in 5-mL fractions for the rats. BAL was centrifuged at $500 \times g$ for 10 min. The cellular pellets from the BAL fractions were pooled and resuspended in 1 mL phosphate-buffered saline (PBS), and total live leukocytes were counted in a Neubauer hemacytometer (Marienfeld) using trypan blue dye (ThermoFisher Scientific) exclusion. Interleukin 1 alpha (IL-1α), macrophage chemotactic protein-1 (MCP-1), tumor necrosis factor-α (TNFα), interferon gamma (IFN-γ), granulocyte–monocyte colony stimulation factor (GM-CSF), and IL-4 concentrations were analyzed in frozen, preserved (−80°C) BAL supernatants by flow cytometry using a bead-based multiplex immunoassay (FlowCytomix™; testing kit materials generously given by eBioscience; assay limited to the BN rat).

Lung Tissue Processing

Immediately after BAL collection, the pulmonary vascular circuit was washed with 2 mM ethylenediaminetetraacetic acid (EDTA) in PBS, injected through the right ventricle, and flushed out through an opening in the abdominal aorta. The cardiopulmonary block was then dissected out and connected to a formalin recirculation system through the tracheal cannula. The lungs were thus inflated and fixed with 10% formalin at 25 cmH_2O intratracheal standard pressure for 22 h. From the inflated, fixed lungs, sagittal slices were cut with a scalpel, placed into standard tissue processor cassettes (ThermoFisher Scientific), and paraffin embedded with the lung midsagittal plane facing the microtome cutting side as per previously established methodology for airway and parenchyma quantitative morphology (Guerassimov et al. 2004; Ramos-Barbón et al. 2005). For this purpose, a 2-mm-thick lateral slice was trimmed and discarded, and the slice generated by sectioning at the lung midsagittal plane was processed for paraffin embedding. From the paraffin blocks, 5-µm-thick microtome tissue sections were stained with hematoxylin and eosin (H&E) for general histopathological assessment, periodic acid–Schiff (PAS) to quantify goblet cells and airway mucus load, and Masson's trichrome to evaluate airway subepithelial fibrosis.

Quantification of Pulmonary Emphysema

Two quantitative morphology methods were employed to measure pulmonary emphysema on H&E-stained sections. Two midsagittal slides per animal, from the right and left lung, respectively, were examined. The lung parenchyma was thoroughly sampled into images that were black/white binarized to discern the alveolar wall tissues from airspaces, and the surface area of the digitally extracted parenchymal tissue was referenced to the sampled surface area to express parenchymal tissue density as a dimensionless percentual index. For the alternative method, we calculated the parenchymal mean linear intercept (MLI), a well-established parameter for the quantitative assessment of pulmonary emphysema on tissue sections (Dunnill 1962; Parameswaran et al. 2006; Robbesom et al. 2003). For this purpose, 15 images were randomly sampled at 200 × magnification from subpleural regions, and a grid with 6 equally distributed horizontal lines and 8 vertical lines was overlaid (Figure S2). The line intercepts with alveolar walls were counted, and MLI was calculated as:

$$\mathrm{MLI} = \frac{V \times Lv + H \times Lh}{Ni},$$

where V is the number of vertical lines, Lv is the length of each vertical line, H is the number of horizontal lines, Lh is the length of each horizontal line, and Ni is the sum of all intercepts. A BX61/BX62 Olympus microscope equipped with a DP70 Olympus

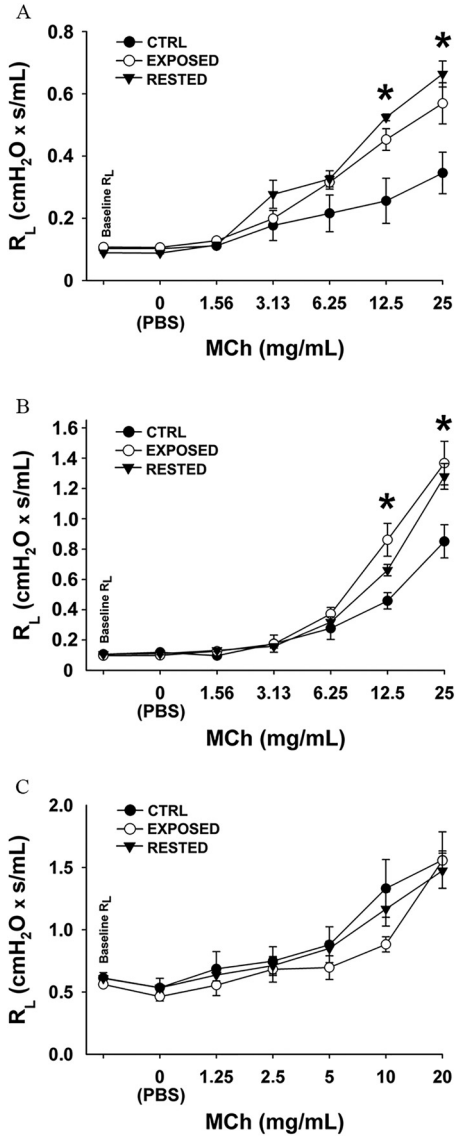

Figure 1. Airway responsiveness to methacholine challenge. The plots represent the pulmonary resistance (R_L) peak after each methacholine (MCh) dose. The Exposed animals inhaled fuel oil–derived VOCs for 2-h sessions, 5 times per week, for 3 wk. The Rested animals were subjected to the same VOC exposure regime followed by a 2-wk washout period. The Control (CTRL) animals had no exposure. These group definitions apply uniformly to the Wistar and Brown Norway rats and the C57BL/6 mice for all subsequent figures and data tables as applicable. R_L values of (A) Wistar rats, (B) Brown Norway rats, and (C) C57BL/6 mice are shown. Error bars represent the standard error of the mean. $^*p < 0.05$ vs. CTRL for both the Exposed and Rested groups. Statistical analysis: one-way analysis of variance (ANOVA) with Fisher's least significant difference (LSD) test for pairwise post-ANOVA comparisons at each MCh concentration level; $n = 6$ for all experimental groups.

camera was used for image capture, and ImageJ software (version 1.47; National Institutes of Health) was used for digital image processing and quantitative procedures.

Detection and Quantification of Apoptotic Structural Alveolar Septal Cells

Apoptotic cells were detected in lung parenchyma by the terminal deoxynucleotidyl transferase dUTP nick end labeling (TUNEL) assay using ApopTag® kits (Millipore) per the manufacturer's instructions. The numerical density of apoptotic alveolar septal cells was calculated by stereology (Hsia et al. 2010), analyzing 10 random fields per animal on 20-μm-thick tissue sections and discarding the cells whose nuclei were in contact with the focal plane corresponding to the microscope slide surface. By this procedure, $TUNEL^+$ alveolar septal cells were counted in the alveolar walls, normalized by cubic millimeter of parenchymal tissue, and expressed as apoptotic cells per cubic millimeter. The reference parenchymal tissue volume was quantitated by digital extraction as for the calculation of pulmonary emphysema. The microscope sample fields were captured with a 40× bright-field objective and yielded a 152,053.08-μm^2 surface area and 3,041,061.69-μm^3 volume upon calibration. Field sampling from one midsagittal right lung microscopy slide per animal yielded appropriate statistical power for the effects detected in the TUNEL-processed specimens and in the CD31, VEGF, CD8, and neutrophil elastase–immunostained preparations (next section).

Immunohistochemical Detection and Quantification of CD31, Vascular Endothelial Growth Factor, CD8, and Neutrophil Elastase

Lung tissue sections were deparaffinized and rehydrated through 5-min baths in xylene (three baths), 100% ethanol (two baths), and 95% and 70% ethanol, and placed in PBS or Tris-buffered saline. High-temperature epitope unmasking was done in Universal Antigen Retrieval Reagent (Abcam) using a 2100 Retriever (Aptum Biologics Ltd.). The tissue sections were then permeabilized in 0.2% Triton-X 100 (Sigma-Aldrich) and blocked with 2.5% goat serum or horse serum (Vector Laboratories) as appropriate. The following primary antibodies (all from Abcam) were used: anti-CD31 rabbit monoclonal EPR17259 at 1:500 dilution (1.2 μg/mL). Anti-VEGF rabbit polyclonal (ab53465) at 1:300 dilution (3.3 μg/mL), anti-CD8 mouse monoclonal OX-8 at 1:200 dilution (5 μg/mL), and anti-neutrophil elastase rabbit polyclonal (ab21595) at 1:200 dilution (5 μg/mL). CD31 immunostaining was selected as a procedure to label endothelial cells, allowing for precise detection of microvasculature down to the capillary level (Pusztaszeri et al. 2006). For CD31 and neutrophil elastase immunostaining, endogenous peroxidase was blocked with BLOXALL® solution (Vector Laboratories), and a goat anti-rabbit IgG secondary antibody with polymerized horseradish peroxidase (ImmPRESS® reagent; Vector Laboratories) was applied. CD31 detection was developed with Vector Novared chromogen, and neutrophil elastase with diaminobenzidine (DAB)–nickel (Vector Laboratories) on respective slide sets. The anti-VEGF and anti-CD8 primary antibodies were followed by *a*) biotinylated goat anti-rabbit IgG and horse anti-mouse IgG secondary antibodies, respectively (both from Vector Laboratories) at 1:200 dilution (7.5 μg/mL); *b*) an alkaline phosphatase avidin–biotin complex (ABC-AP, Vector Laboratories); and *c*) Vector® Red chromogen (Vector Laboratories). All second-step reagents (ImmPRESS® reagent and biotinylated secondary antibodies) were adsorbed in 10% normal rat serum (STEMCELL Technologies). Chromogen development was followed by hematoxylin QS counterstain (Vector Laboratories), dehydration through two 100% ethanol and three xylene baths, and permanent mounting with VectaMount medium (Vector Laboratories).

The volume density (dimensionless) of CD31-immunostained endothelium within the alveolar walls was calculated by digital signal thresholding and extraction and referenced to the digitally extracted parenchymal tissue, similar to the procedure referred for the calculation of parenchymal volume density in the quantification of emphysema, but using a 60× oil immersion objective for image capture in this case. The numerical density of $VEGF^+$ and $CD8^+$ cells was calculated by cell counting normalized by cubic millimeter of parenchymal tissue, similar to the numerical

density of apoptotic alveolar septal cells. All calculations were also done with ImageJ software (version 1.47).

Data Analysis

Data distributions are represented by the mean and standard error. Statistical significance was analyzed by one-way analysis of variance (ANOVA) followed by post hoc Fisher's least significant difference test or Games-Howell test for unequal variances. Student's *t*-test was used where appropriate for two-group independent comparisons. Inferences on the size of effects are reported as mean increment [mean difference (95% confidence interval of the mean difference)]. A *p*-value of less than 0.05 was considered statistically significant. SPSS statistical software was employed (version 16.0; IBM Corp.).

Results

Evaluation of Airway Responsiveness to Methacholine Challenge

Wistar and BN rats and the C57BL mice were subjected to R_L determinations upon MCh challenge *in vivo* for the Control, Exposed, and Rested groups, respectively, as specified in the study design. R_L curves are plotted in Figure 1, and the corresponding numerical data and exact *p*-values are shown in Table S2. Both the Wistar and BN rats showed airway hyperresponsiveness to MCh in the exposed groups, defined as per significant differences in R_L at the two highest MCh doses ($p < 0.05$ over the Control group for the 12.5 and 25 mg/mL MCh doses, respectively; Figure 1A,B). The R_L curves were similar for both rat strains in the Rested groups, which reflected that airway hyperresponsiveness persisted despite discontinuing VOC exposure. Conversely, no changes in respiratory parameters were found in the C57/BL6 mice at any data cutoff (Figure 1C).

Bronchoalveolar Lavage Analyses and Airway Histopathology

Total BAL cell counts (Figure 2; numerical data and *p*-values in Table S3) did not show any significant differences among the experimental groups for any of the rat strains or the C57BL mouse. The BN rat showed a tendency toward a progressive increase in total BAL cells through the VOCs inhalation and washout periods, which did not reach statistical significance ($p = 0.22$ in the Exposed group and $p = 0.09$ in the Rested group vs. the Control animals). Since this trend in the BN rat was close to significance in the Rested group, we performed a multiplex cytokine analysis in the BAL fluid of this strain, which did not show any significant difference supportive of inflammatory activity in the Exposed or Rested groups. The cytokine analysis battery included IL-1α, MCP-1, TNFα, IFN-γ, GM-CSF, and IL-4 (Figure 2D). This analysis, performed with a test kit sample, was limited to the BN rat, selected based on its BAL leukocyte counts profile. Because of the spread variability of the cytokine distributions obtained and its null outcome, we estimated a very low probability of obtaining any informative data from the Wistar rat and the C57BL mouse, and we deemed it not cost-effective to pursue such analyses.

A systematic scan of the H&E-stained tissue sections did not reveal any pathological findings in the conducting airways. Notably, no airway inflammation or remodeling were found. Representative sections of intrapulmonary airways are shown in Figure 3, where it can be seen that VOCs inhalation did not lead to any detectable inflammatory infiltrates or signs of airway remodeling as compared with controls in the BN rats (Figure 3A–C), Wistar rats (Figure 3D–F), or C57BL/6 mice (Figure 3G–I). PAS staining did not reveal any alterations of mucus-producing cells or overall epithelial mucous load, and we did not observe differences in extracellular matrix deposition or abnormal patterns such as subepithelial fibrosis in the Masson's trichrome–stained specimens (Figure 4). Overall, the analyses on the cellular and fluid BAL fractions and the histopathological

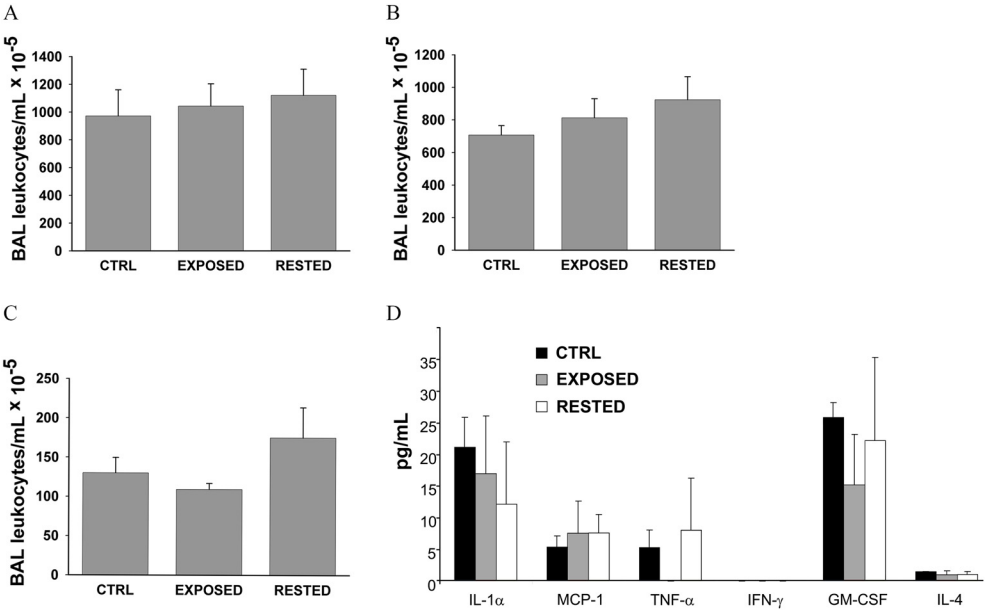

Figure 2. Bronchoalveolar lavage (BAL) analysis. Total BAL leukocytes were counted at the end of VOCs exposure (Exposed group) and after a 2-wk washout (Rested group) vs. Control animals (CTRL). BAL leukocyte counts are shown for (A) the Wistar rat, (B) Brown Norway rat, and (C) C57BL/6 mouse. (D) BAL cytokine concentrations measured in the Brown Norway rat groups by a bead-based multiplex flow cytometry immunoassay. Minimum detectable levels were 8.5 pg/mL for interleukin 1 alpha (IL-1α), 0.5 pg/mL for macrophage chemotactic protein 1 (MCP-1), 4.3 pg/mL for tumor necrosis factor-α (TNFα), 8.3 pg/mL for interferon gamma (IFN-γ), 5.0 pg/mL for granulocyte–monocyte colony stimulation factor (GM-CSF), and 0.3 pg/mL for IL-4. Graph bars represent mean and standard error of the mean in all plots. One-way analysis of variance (ANOVA) with Fisher's least significant difference (LSD) test for pairwise post-ANOVA comparisons; $n = 6$ for all experimental groups.

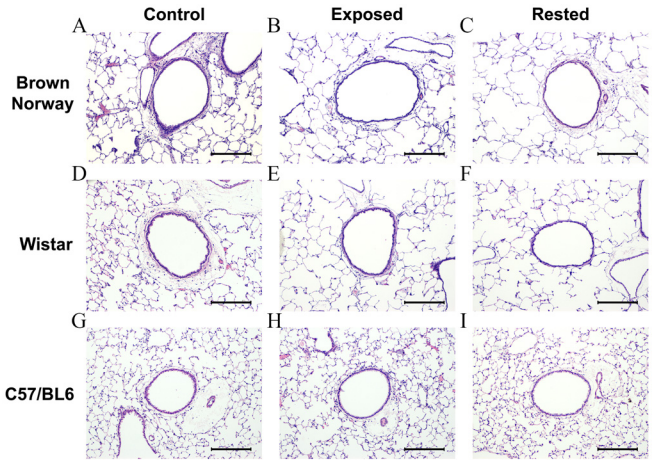

Figure 3. Airway histopathology in hematoxylin and eosin–stained tissue sections. Micrographs show representative cross-sectioned airways from the respective strains and experimental groups as indicated. Scale bars: 200 μm.

examination of stained tissue sections ruled out any detectable signs of persistent airway inflammation and remodeling underlying the sustained airway hyperresponsiveness. The experimental design did not aim at detecting possible acute lung inflammation during early VOC exposure.

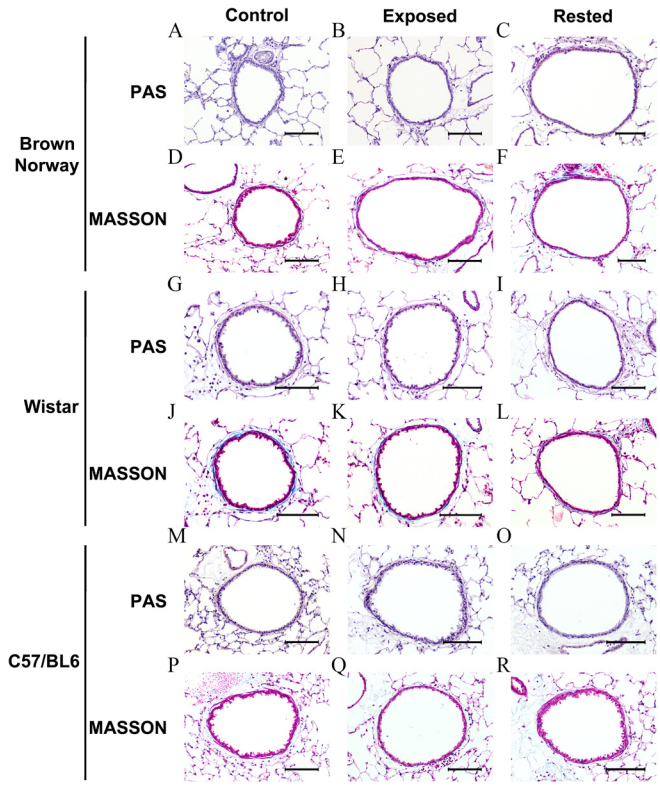

Figure 4. Periodic acid–Schiff (PAS) and Masson's trichrome staining. Lung tissue sections were stained with PAS to identify goblet cells and evaluate the overall airway epithelial mucus load. Masson's trichrome was employed to evaluate extracellular matrix deposition. The panels show representative cross-sectioned airways for the respective stainings, animal strains, and experimental groups as indicated. No pathological alterations were identified in terms of goblet cell hyperplasia or hypertrophy, overall epithelial mucus load, or subepithelial fibrosis as a result of volatile organic compounds (VOCs) inhalation. Scale bar: 100 μm.

Detection and Quantitative Analysis of Pulmonary Emphysema

On histopathological examination, the Wistar and BN rats showed pulmonary emphysema that predominantly affected the most peripheral parenchymal regions in a subpleural location in both the Exposed and Rested groups (Figure 5A–F). Quantitative morphology by the digital extraction and MLI methods jointly showed a progression whereby the parenchymal tissue density was significantly decreased at the end point of exposure, and further tissue destruction occurred during the washout period (Figure 5G–J; quantitative data and *p*-values given in Tables S4 and S5).

The C57BL/6 mice did not show any changes in the lung parenchyma on histopathological examination, whether upon exposure or after the washout, compared to the Control group (Figure S3).

Similar to the airways, a thorough scan of the lung parenchyma did not reveal any inflammatory infiltrates. To reassure the absence of neutrophil involvement associated with the development of emphysema, we immunostained neutrophil elastase in the rat lung specimens. Figure S4 shows examples of circulating neutrophils as an internal staining control. We found such neutrophils in limited blood remnants that were retained in some vessels despite the pulmonary vascular circuit wash performed during dissection. All experimental groups were devoid of extravascular neutrophils infiltrating any tissue structures.

Detection and Quantification of Structural Alveolar Septal Cell Apoptosis

In search of a mechanism underlying the development of pulmonary emphysema, we detected and quantified alveolar septal cell apoptosis in the rats. Both the Wistar and BN rat strains showed a significant increase in the frequency of $TUNEL^+$ alveolar septal cells in the Exposed groups vs. the respective Control groups, and this effect was maintained after the washout period in the Rested groups (Figure 6B,C and Figure 7; Table S6).

Frequency of $CD8^+$ T Cells in the Lung Parenchyma

To explore a possible role of $CD8^+$ T cells as potential inducers of alveolar septal cell apoptosis through cytotoxicity, we quantified the numerical density of immunostained $CD8^+$ cells in the parenchyma (Figure 8; numerical data and *p*-values given in Table S7). BN control rats had a higher baseline frequency of $CD8^+$ cells compared with Wistar rats. VOCs inhalation did not lead to consistent changes in the Exposed groups, but there was a significant decrease of $CD8^+$ cell numerical density in the Rested groups of both strains.

Analysis of Parenchymal Microvascular Response

To analyze whether the development of emphysema was associated with alterations of the parenchymal microvasculature, we labeled the endothelium by CD31 immunostaining. The general CD31 immunostaining pattern on different lung structures is shown in Figure S5. Consistent with previous reports (Pusztaszeri et al. 2006), the CD31 signal accurately delineated the parenchymal capillary network and allowed us to quantify its volume density within the alveolar walls. Upon overall microscopy examination, we observed a noticeable difference in CD31 signal density between the subpleural regions and the rest of the lung parenchyma in the animals of the Exposed and Rested groups. This finding prompted us to acquire two separate sampling sets for quantitative morphology: central and subpleural parenchyma (Figure 9; numerical data and *p*-values given in Table S8). The $CD31^+$ endothelium volume density was homogeneous across the parenchymal regions in the Control animals within the Wistar and BN strains. The BN control rats showed

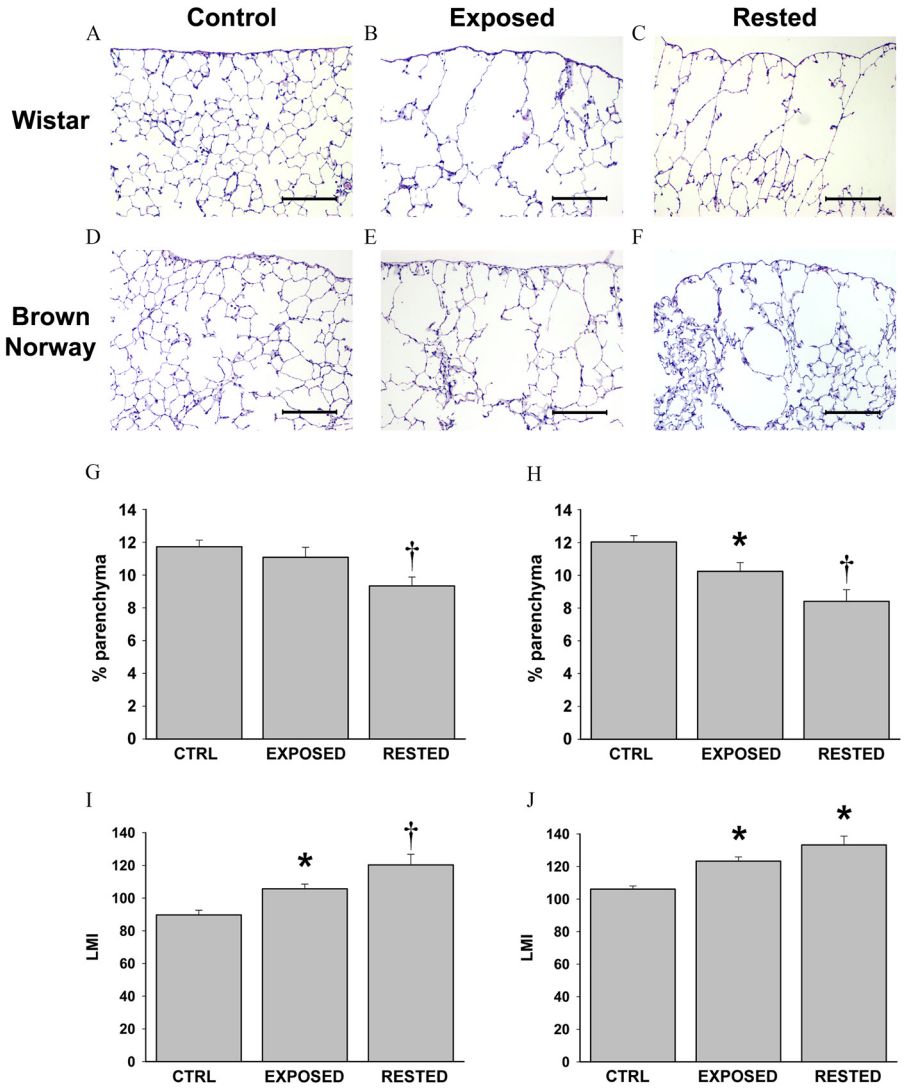

Figure 5. Effect of VOCs inhalation on lung parenchyma. The micrographs (A–F) show hematoxylin and eosin–stained lung sections capturing the subpleural region of lung parenchyma. All tissue sections are oriented showing the pleura on top. The panels correspond to the Wistar and Brown Norway rats and the respective experimental groups, as indicated. Pulmonary emphysema is seen as a decreased number of alveolar walls due to tissue destruction. The bar graphs (G–J) represent mean and standard error values for the corresponding quantitative morphology measurements by digital parenchymal extraction (G–H) and mean linear intercept (MLI) method (I–J) for the Wistar rat (G,I) and Brown Norway rat (H,J), respectively. Scale bar: 200 μm. $^{*}p < 0.05$ vs. Control (CTRL) group. $^{\dagger}p < 0.05$ vs. both Control and Exposed groups. One-way analysis of variance (ANOVA) with Fisher's least significant difference (LSD) test for pairwise post-ANOVA comparisons; $n = 6$ for all experimental groups.

a tendency to lesser CD31 density than their Wistar counterparts, which reached significance in the subpleural region ($p = 0.029$), attributable to a constitutive interstrain difference. In the Exposed groups, the fuel oil VOCs inhalation led to a significant decrease of the CD31 volume density in both the central and subpleural parenchyma, this effect being drastic in the latter region. This outcome was comparable between both rat strains. In the Wistar rat, the Rested group showed a significant recovery of CD31 volume density within the remnant alveolar walls of the subpleural region, which morphologically generated a peculiar budding sprout aspect. The Rested BN rats did not show such significant recovery.

The findings from the CD31-labeled microvasculature analysis and the reported increase of VEGF in exhaled breath condensate from subjects involved in the *Prestige* spill decontamination (Rodríguez-Trigo et al. 2010) led us to immunostain VEGF. As in previously reported lung VEGF expression profiling (Berse et al. 1992; Medford et al. 2009), we found the VEGF signal predominantly located in alveolar septal cells and alveolar macrophages. We quantified the numerical density of $VEGF^{+}$ cells in the alveolar walls (Figure 10; numerical data and *p*-values given in Table S9). Similar to CD31, there was an interstrain difference where the control BN rats had a significantly lower VEGF expression profile that the control Wistar rats ($p < 0.001$). Since the immunostaining batches comprised a balanced presence of slides from all experimental groups of both rat strains together, and the timing of reagent incubations, including chromogen development, was sequenced to be strictly systematic on a per-slide basis, we deem the observed interstrain differences not attributable to interference related to batch staining. In both strains, the Exposed groups had a significant, strong inhibition of VEGF expression that remained flat in the Rested groups.

Discussion

The field research conducted after the *Prestige* tanker and the *Deepwater Horizon* oil rig disasters left a knowledge gap about the pathophysiological processes that may have underlain the

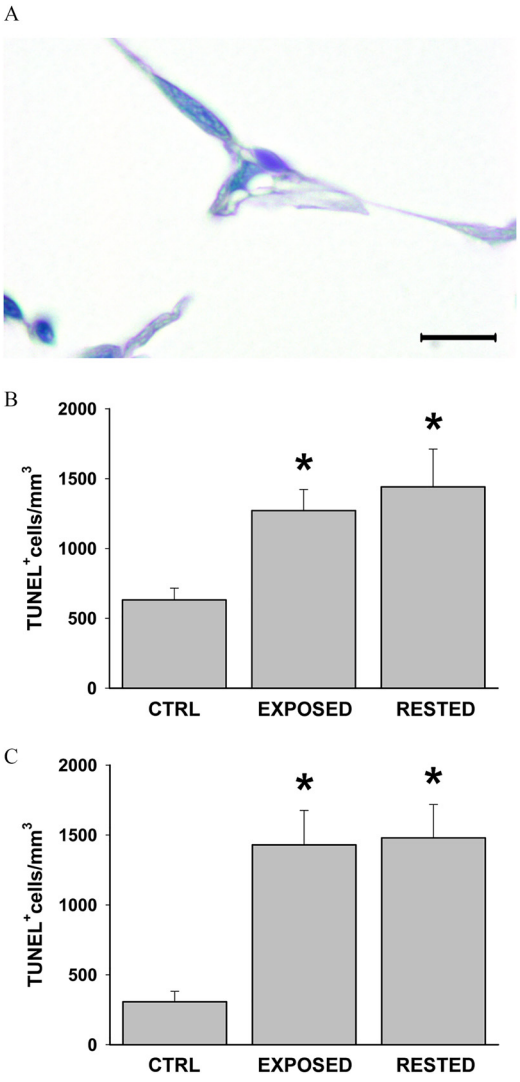

Figure 6. Detection of apoptotic alveolar septal cells in rat lung parenchyma. Apoptosis was detected by the terminal deoxynucleotidyl transferase dUTP nick end labeling (TUNEL) technique on lung tissue sections. (A) Detail of an apoptotic alveolar septal cell, likely a type I pneumocyte, identified by its purple-stained nucleus with condensed chromatin. The bar graphs show the quantitative morphology data on the frequency of alveolar septal TUNEL$^+$ cells for the Control, Exposed, and Rested experimental groups in (B) the Wistar rat, and (C) the Brown Norway rat. Scale bar: 10 μm. $^*p < 0.05$ vs. Control (CTRL) group. One-way analysis of variance (ANOVA) with Fisher's least significant difference (LSD) test for pairwise post-ANOVA comparisons; $n = 6$ for all experimental groups.

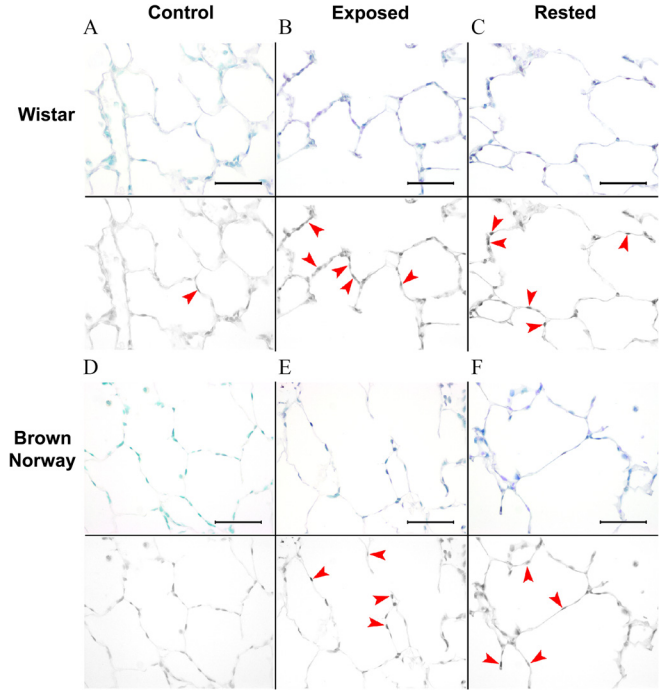

Figure 7. Distribution of apoptotic alveolar septal cells. For quantitative morphology, the terminal deoxynucleotidyl transferase dUTP nick end labeling (TUNEL$^+$) alveolar septal cells were identified through high-resolution field sampling. The images shown here are low-magnification micrographs to illustrate the overall frequency and distribution of apoptotic alveolar septal cells in wide microscopy fields. The micrographs represent the Wistar and Brown Norway rat strains and the respective experimental groups, as indicated. For each rat strain and experimental group, the upper image is a direct micrograph, and the lower image is a grayscale replica where the location of apoptotic cells, as per identification at high magnification, is pinpointed (red arrows). Scale bar: 50 μm.

lasting respiratory effects, observed years after the respective spills, in the catastrophe response crews exposed to VOCs inhalation (Gam et al. 2018a, 2018b; Rodríguez-Trigo et al. 2010; Zock et al. 2011, 2007). Here, we aimed at a mechanistic insight on respiratory system damage by developing an experimental model of fuel oil–derived VOCs inhalation mimicking the *Prestige* catastrophe. The system setup involved interdisciplinary collaboration among various entities to achieve challenging technical goals. The study fuel oil was blended at a research refinery facility based on known parameters from the *Prestige* tanker payload. The ad hoc production of a VOCs-generating and decontamination exhaust system and its coupling to a standardized rodent inhalation tower involved research, manufacturing, and testing by a specialized engineering firm. VOC sampling and profiling at the equipment inhalation ports and data matching with field measurements from the actual *Prestige* spill at the human exposure zones were performed by a gas spectrometry analytics facility. Ultimately, the data production procedures were done by a respiratory research unit branched into two hospital research institute sites. Laboratory modeling of an environmental catastrophe implies limitations, and some assumptions are unavoidable. We analyzed BTEX concentrations in the air from the exposure tower ports to provide our best accuracy on what precisely the animals were breathing, yet the comparability of these data with the field fuel oil analyses is limited by several factors as detailed in the "Methods" section. The extent to which the VOCs release in this model reflects the human exposure mostly relies on the customized synthesis of the model fuel oil based on the *Prestige* payload specifications. Another limitation to extrapolate our data to the human experience is the inability to analyze any gender-related differences, since only female mice and rats were employed in the experiments. Since the primary outcome that we aimed to reproduce was airway hyperresponsiveness, and our *a priori* expectations were on airway inflammatory disease, we opted for employing female animals as often done in asthma models. The overall asthma prevalence and mortality are higher in women (Akinbami et al. 2012; Moorman et al. 2012), and this epidemiological observation may have historically tilted rodent asthma models towards the frequent use of female animals, yet without generating much evidence on possible gender-related differences in the outcomes of such models. More recent comparative studies in murine asthma reported significantly higher allergen-specific IgE, Th2 cytokines, eosinophilic inflammation, and airway hyperresponsiveness in the female animals (Blacquière et al. 2010; Takeda et al. 2013). Finally, the sequence of procedures performed

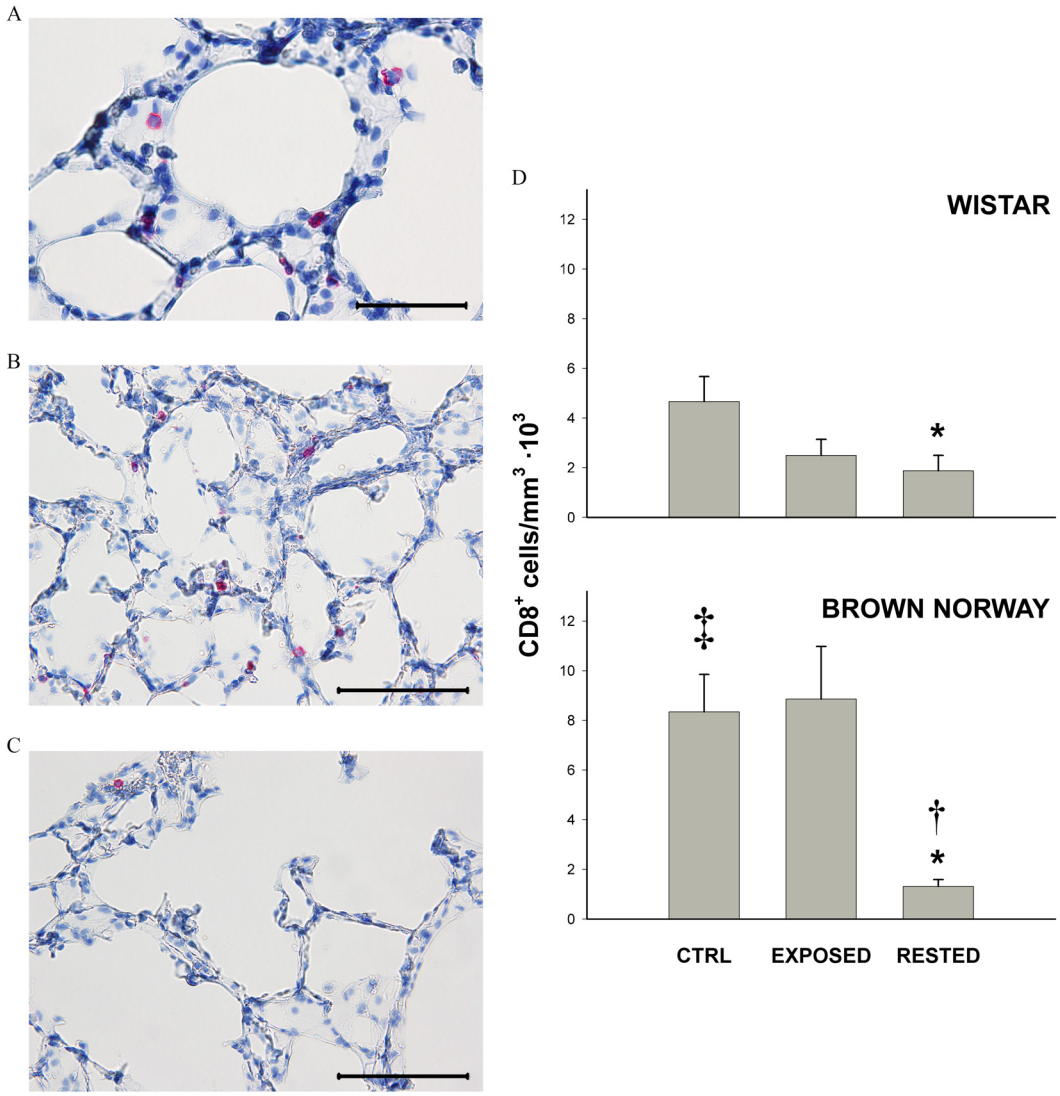

Figure 8. Quantification of $CD8^+$ T cells in lung parenchyma. $CD8^+$ cells were immunostained (red signal) and their numerical density quantified in the alveolar walls. Counterstain: hematoxylin QS. (A) Example of a high-magnification field as employed for quantitative morphology. The micrograph corresponds to a control Wistar rat. (B) Lower-magnification capture encompassing a large parenchyma field, where a number of $CD8^+$ cells can be identified. The image, from another control Wistar rat, is representative to provide a visual sense of the frequency of $CD8^+$ T cells in control animals. (C) Example from the Wistar Rested group showing a wide field under the same magnification as in (B). A number of fields sampled from the Rested groups of both rat strains did not contain any $CD8^+$ cells. The image shown here has intentionally captured one $CD8^+$ cell as a reference, visible in the upper-left quadrant. (D) Numerical density of $CD8^+$ T cells in the alveolar walls. $^*p < 0.05$ vs. Control (CTRL). $^\dagger p < 0.05$ vs. Exposed. Scale bar: 50 μm in (A); 100 μm in (B,C). One-way analysis of variance (ANOVA) with Fisher's least significant difference (LSD) test for pairwise post-ANOVA comparisons; $n = 6$ for all experimental groups. $^\ddagger p < 0.05$ vs. Wistar for independent interstrain group comparison (Student's *t*-test).

in the same animals may have involved some confounding risk due to carryover effects. This uncertainty particularly applies to the obtention of biological specimens after ending pulmonary function testing with MCh challenges under invasive mechanical ventilation. Although such a methodological sequence is often performed in experimental asthma models and has been in extended use (Ramos-Barbón et al. 2004), a lack of any effects of the *in vivo* invasive procedures on the biological samples collected subsequently is not warranted.

To explore the suitability of rodent species to model the respiratory effects recorded in humans, we performed experiments in mice and rats. The single mouse strain tested, C57BL/6, failed to represent *in vivo* the primary functional outcome obtained from humans, airway hyperresponsiveness to MCh challenge, whereas both rat strains, Wistar and BN, did reproduce such an outcome comparably. The mouse has been extensively employed for inhalational studies, but only limited comparative work across species has been published, with a homogeneous response not always obtained. The rat has been reported to be more sensitive than the mouse to low-respiratory-tract effects of 1,6-hexamethylene diisocyanate inhalation (Pauluhn 2008). Anatomical and physiological differences exist in the respiratory tract and pulmonary vasculature between the mouse and rat, which may introduce complexity factors for respiratory disease modeling. In our study, given that both rat strains yielded a comparable output for the relevant outcomes detected, we did not pursue further investigations across different mouse strains following the null response of the C57BL/6.

Both Wistar and BN rats showed airway hyperresponsiveness at the end of the exposure period, which was maintained without significant variation after the washout. This finding suggests a persistent disease mechanism regardless of the exposure washout, which is also independent from the Th1 vs. Th2 constitutive immunological

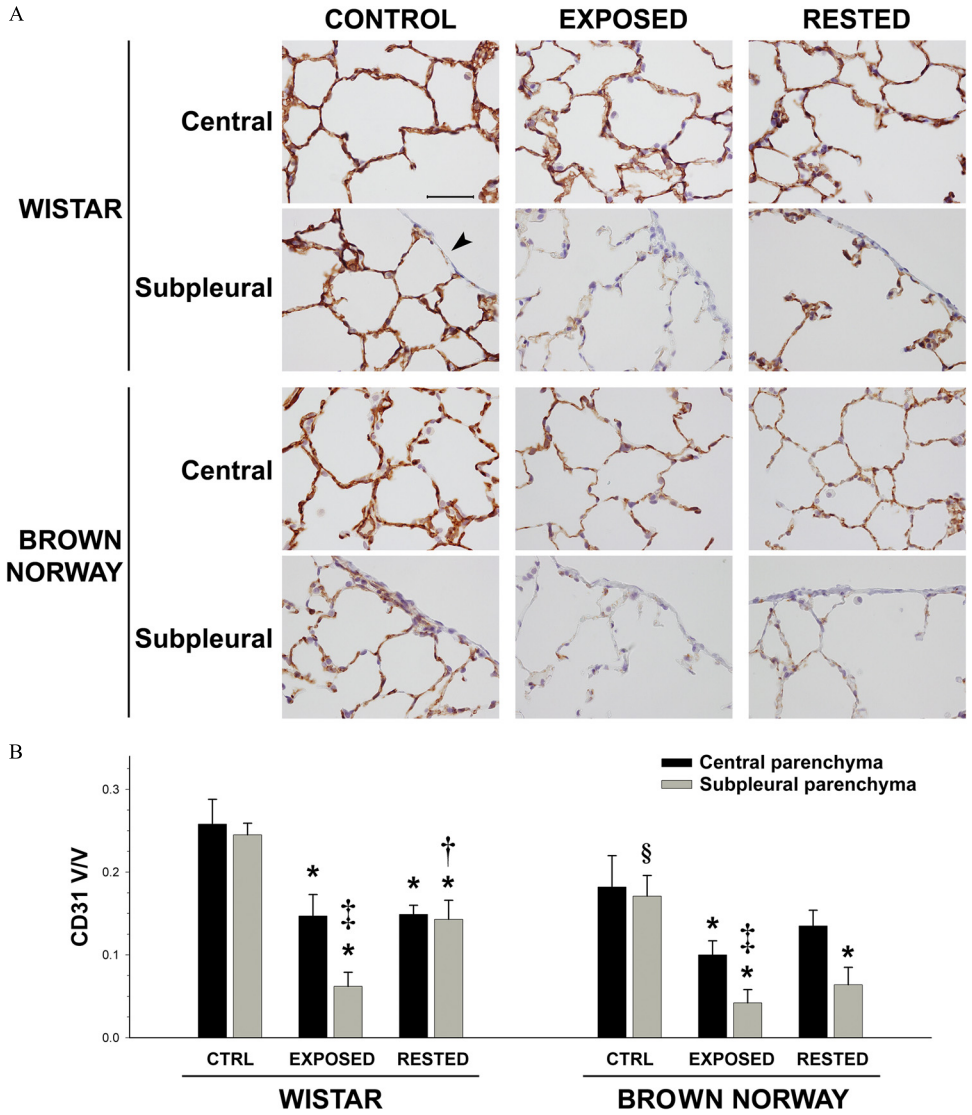

Figure 9. Immunostaining and quantitative morphology of parenchymal microvasculature. Lung endothelium was labeled by CD31 immunostaining, and its volume density (V/V, dimensionless) in the alveolar walls was quantified. Due to noticeable differences in the CD31 signal density between peripheral (subpleural) and central parenchymal regions, two separate sampling sets were acquired and analyzed for quantitative morphology, respectively. (A) Representative images of CD31-immunostained (brown signal) parenchyma from the central and subpleural regions for the Control, Exposed, and Rested groups of the Wistar and Brown Norway rat strains, as indicated. Counterstain: hematoxylin QS. The arrow in the left-hand image of the Wistar subpleural set indicates the visceral pleura. To facilitate image interpretation, the pleura was captured in the approximate same position in all subpleural images. The scale bar (50 μm) in the upper-left panel applies to all micrographs. (B) Quantitative morphology of CD31-immunostained endothelium V/V for the experimental groups, parenchymal regions, and rat strains, as indicated. $^{*}p < 0.05$ vs. Control. $^{\dagger}p < 0.05$ vs. Exposed. $^{\ddagger}p < 0.05$ vs. central parenchyma, intragroup. One-way analysis of variance (ANOVA) with Fisher's least significant difference (LSD) test for pairwise post-ANOVA comparisons; $n = 6$ for all experimental groups. $^{\S}p < 0.05$ vs. Wistar for independent interstrain group comparison (Student's *t*-test).

background of the strains. Fuel oil exposure did not lead to any significant changes in airway histopathology. A thorough scan of the H&E-stained and neutrophil elastase–immunostained tissue sections did not detect any traces of airway inflammatory infiltrates nor signs of structural remodeling of the airway wall. PAS staining did not reveal goblet cell hypertrophy or hyperplasia nor increased mucus production, and the Masson's trichrome–stained specimens did not show any differences in extracellular matrix deposition. Furthermore, total BAL cellularity and cytokine contents in BAL supernatant were not altered. In all, the data ruled out any detectable airway disease in the form of inflammation, increased mucus production, or remodeling. We also did not find signs of inflammation at other locations in the lung tissue sections, such as perivascular or in the parenchyma. VOCs cannot act as antigens due to their low molecular weight but may still initiate an adaptive immune response by acting as haptens through carrier protein binding as reported for occupational exposure to toluene, one of the VOCs released by the fuel oil blend employed in our study (Karol 1983). In the absence of an adaptive immune response, VOCs may interact with innate immunity pathways through contact with the airway epithelium and elicit inflammation, as described for reactive airways dysfunction (Vincent et al. 2017). Given the various possibilities by which VOCs may potentially activate immune system pathways, our working hypothesis was that airway hyperresponsiveness was underlain by an inflammatory response as generally is the case in airway disease. The inflammatory silence revealed by our data in all lung compartments was, therefore, a puzzling outcome to us. In the human investigations, 8-isoprostane, VEGF, and bFGF were increased in exhaled breath condensate, but no evidence of inflammatory activity was found

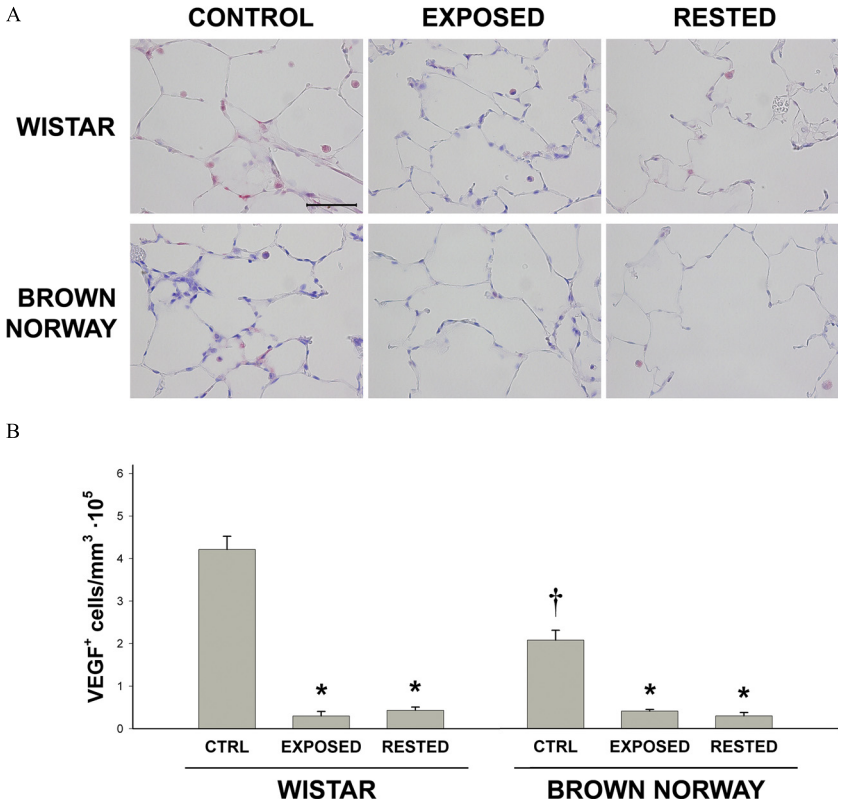

Figure 10. Vascular endothelial growth factor (VEGF) immunostaining and quantitative morphology. (A) VEGF immunostaining (red signal) in the experimental Control, Exposed, and Rested groups of the Wistar and Brown Norway rats, as indicated. Counterstain: hematoxylin QS. The scale bar (50 μm) in the upper-left panel applies to all micrographs. (B) Numerical density of $VEGF^+$ cells in the alveolar walls of the respective experimental groups and rat strains, as indicated. $^*p < 0.05$ vs. Control. One-way analysis of variance (ANOVA) with Fisher's least significant difference (LSD) test for pairwise post-ANOVA comparisons; $n = 6$ for all experimental groups. †$p < 0.05$ vs. Wistar for independent interstrain group comparison (Student's *t*-test).

as per cytokine analysis (Rodríguez-Trigo et al. 2010). It is noteworthy that our study design did not include any group aimed at analyzing acute respiratory tract inflammation at an early-exposure time point. Therefore, our study cannot rule out the possibility of an early inflammatory response with subsequent down-regulation. Part of the previous work on the respiratory system effects of VOCs inhalation from oil spills focused on acute effects (Alexander et al. 2018; Campbell et al. 1993; Janjua et al. 2006; Lyons et al. 1999; Morita et al. 1999), yet there is a significant knowledge gap on the inflammatory response associated with such outcomes. Such studies have reported symptom descriptions, with few collecting spirometric data, blood hematology and biochemistry, or exposure analytes in urine, and did not attempt to gain insights on the biological mechanisms of the acute respiratory response through assessments of respiratory tract inflammation. Similarly, data on persistent biological mechanisms at a late stage after exposure, such as in the time frame of the studies that followed the *Prestige* tank wreckage, are very limited (Rodríguez-Trigo et al. 2010).

We unexpectedly found pulmonary emphysema, with a particular and unusual pattern of subpleural distribution, developed by both the Wistar and BN Exposed groups. Such emphysema was present at the end-of-exposure cutoff, and the quantitative data suggest further progression by the end of the washout period in the Rested groups. On a per-individual assessment basis, all exposed rats were affected. This finding suggests an explanation for airway hyperresponsiveness in the absence of concomitant inflammation on the basis of known pulmonary mechanics. The destruction of alveolar walls decreases the elastic recoil of the lung parenchyma and facilitates airway narrowing upon a bronchoconstrictive stimulus (Cheung et al. 1997). This mechanism has been proposed to contribute to airway narrowing in chronic obstructive pulmonary disease (COPD) (Koyama et al. 1996; Yang and Lin 2010), although the usual centrilobular distribution of emphysema directly affects the airway alveolar attachments in COPD, and airway inflammation is often present (Verhoeven et al. 2000). To verify the presence of a biological mechanism driving pulmonary emphysema, we performed *in situ* detection of apoptosis by the TUNEL technique on the tissue sections. Quantitative morphology revealed a baseline frequency of apoptotic alveolar septal cells in the control animals, attributable to physiological cell turnover and consistent with previous reports on nonsmoker subjects (Kasahara et al. 2001; Majo et al. 2001) and nonexposed animals in rat models of cigarette smoke-induced emphysema (Kasahara et al. 2000; Li et al. 2017). We found significantly increased numbers of apoptotic alveolar septal cells in the exposed animals of both rat strains, which persisted after the washout. Overall, the data suggest that the inhaled fuel oil–derived VOCs mainly interacted with the lung tissues at the most distal level, regionally affecting the peripheral parenchyma through mechanisms that may not involve inflammation. In several animal models of COPD, emphysema developed despite a noticeable absence of pulmonary inflammation, suggesting that apoptosis of alveolar wall cells is sufficient to cause emphysema without the formation of inflammatory infiltrates (Demedts et al. 2006). $CD8^+$ T cells have been reported to be increased in the lung parenchyma of COPD subjects, not forming apparent inflammatory infiltrates, and $CD8^+$ T-cell-mediated cytotoxicity has been proposed as a mechanism inducing apoptosis of alveolar wall cells (Majo et al. 2001; Saetta et al. 1999). Contrary to this proposed mechanism, our $CD8^+$ T-cell immunostaining and quantification yielded inconclusive data in the

Exposed groups and showed a marked decrease in the Rested groups for both rat strains. It is unclear whether the $CD8^+$ T-cell decrease in the Rested groups may be part of a homeostatic mechanism to inhibit overall cell-mediated cytotoxicity. Previous studies on humans (Tanabe et al. 2012; Mohamed Hoesein et al. 2013) and COPD animal models (Wright et al. 1994; March et al. 2006) demonstrated the persistence or progression of emphysema after cessation of exposure to cigarette smoke but did not attempt to analyze the biological response of the parenchyma to injury interruption once emphysema was established. An alternative mechanism inducing alveolar septal cell apoptosis in our fuel oil VOCs exposure model may be DNA damage, which was detected in blood cells of subjects involved in the handling of oil-contaminated birds from the *Prestige* spill (Laffon et al. 2006). DNA damage has been pointed out as a mechanism inducing apoptosis of alveolar structural cells, leading to pulmonary emphysema (Demedts et al. 2006; Morissette et al. 2009). Airflow dynamics during breathing may have favored higher and more lasting VOC concentrations in the most peripheral regions of the lung parenchyma, where a critical threshold of DNA damage may have been surpassed. One open question regards the mechanisms sustaining alveolar septal cell apoptotic activity and the progression of emphysema after the exposure washout. The finding of increased levels of 8-isoprostane in exhaled breath condensate of the exposed subjects 2 y after the exposure (Rodríguez-Trigo et al. 2010) is most probably an indicator of persistent oxidative stress in the pulmonary milieu. Pulmonary emphysema has been proposed to be proinflammatory by itself (Tokairin et al. 2008), which suggests the hypothesis that, following its induction by VOCs exposure, the persistence of cumulative DNA damage is aided by further tissue stress factors to maintain increased alveolar septal cell apoptosis as a self-sustaining condition.

The involvement of apoptosis in the pathogenesis of pulmonary emphysema affects both principal types of structural alveolar septal cells, i.e., type I pneumocytes and endothelial cells (Imai et al. 2005; Kasahara et al. 2001; Segura-Valdez et al. 2000). Endothelial damage through apoptosis may indeed be an important driving force in the development of emphysema (Demedts et al. 2006). For this reason, we analyzed the volume density of CD31-immunostained endothelium in the alveolar walls. Consistent with the peripheral emphysema pattern in our model, the endothelium volume density was severely reduced in the subpleural parenchymal regions. The quantitative data also revealed, to a lesser degree, a significant decrease of endothelium density in the otherwise apparently unaffected central parenchyma. Remarkably, the Wistar Rested group showed significant re-endothelization of the remnant alveolar walls in the severely affected subpleural regions. This finding does not plausibly suggest an emphysema repair mechanism but may reflect a regenerative response aimed at some functional gas exchange recovery of the alveolar wall remnants after the emphysema-inducing insult has ceased. The strain difference preventing the BN rat from developing such endothelium recovery is unclear. To our knowledge, the possibility of postinjury microvascular regeneration in emphysematous lungs has not been hypothesized, whether in ex-smoker COPD subjects or animal models. We observed strong inhibition of VEGF expression in the Exposed and Rested groups of both strains. Significantly reduced VEGF expression was shown in emphysematous COPD subjects (Kasahara et al. 2001), and the VEGF receptor 2 was decreased in association with alveolar cell apoptosis in murine cigarette smoke–induced emphysema (Bartalesi et al. 2005). Also in the mouse, lung-targeted ablation of the *VEGF* gene (Tang et al. 2004) or blockade of the VEGF receptor (Kasahara et al. 2000; Tuder et al. 2003) were sufficient to elicit apoptosis of alveolar septal cells and the development of emphysema. The finding of VEGF inhibition in our fuel oil VOCs–Exposed groups is therefore coherent and supports the idea of apoptosis-driven endothelial damage and development of emphysema in the absence of inflammation. However, there is no obvious interpretation of the flat persistence of reduced VEFG expression in the Rested groups, particularly considering the septal endothelium recovery seen in the Wistar rats, which suggests the involvement of alternative, undetermined pathways with significant capacities for the maintenance of the alveolar structures. The Rested groups' data also mismatch the VEGF increases reported in exhaled breath condensate from the *Prestige* VOCs-exposed subjects (Rodríguez-Trigo et al. 2010).

In summary, experimental inhalational exposure of rats to VOCs released by a fuel oil mimicking the *Prestige* tanker spill induced airway hyperresponsiveness, alveolar septal cell apoptosis, and pulmonary emphysema with parenchymal microvascular endothelial damage in the absence of inflammation and any signs of airway disease. All effects were present at the end of a 3-wk exposure period and persisted with emphysema progression after a 2-wk washout, suggesting a self-sustained disease mechanism. The presence of airway hyperresponsiveness after the washout, with undetectable signs of concomitant inflammatory activity, suggests an analogy with the data from the studies conducted on human subjects in the affected areas with a 2-y lapse after the catastrophe. The pulmonary emphysema, with an unusual pattern of distribution over the most peripheral areas of the lung parenchyma, suggests a lung mechanics explanation for the noninflammatory airway hyperresponsiveness. Although with limited evidence, the studies on humans, combined with the outcomes from our experimental model, allow us to speculate that DNA damage and oxidative stress may have been the driving mechanisms leading to alveolar septal cell apoptosis and the development of a pulmonary emphysema pattern different from typical cigarette smoke–induced emphysema in its distribution and pathophysiology. Our experimental model, in line with the available human data, supports the idea that inhalational exposure to VOCs from fuel oil spill catastrophes may elicit persistent respiratory disease and provides a plausible postulate for the pathophysiological mechanisms involved. The data warrant effective respiratory protection measures and provide suggested guidance for clinical investigations and follow-up upon potential spill incidents in the future.

Acknowledgments

This work was funded by the Xunta de Galicia (grants 07CSA048916PR and INCITE07PXI916208E), Sociedad Española de Neumología y Cirugía Torácica (SEPAR) (grant 05/107), and Instituto de Salud Carlos III (grants PI08/1822, FI07/00399, and FI05/00171) of Spain. The work was surveyed by the Instituto Tecnológico de Galicia (ITG) as an independent observer and promoter entity (EPO). We thank the Repsol Technology Center in Madrid (Spain) for kindly synthesizing the fuel oil employed; Electro-Medical Measurement Systems (EMMS) engineers, especially Peter Connor, for the efforts in researching and manufacturing the experimental exposure equipment; and the Central Research Support Services of Universidade da Coruña for their guidance and gas spectrometry analysis.

References

Akinbami LJ, Moorman JE, Bailey C, Zahran HS, King M, Johnson CA, et al. 2012. Trends in asthma prevalence, health care use, and mortality in the United States, 2001–2010. NCHS Data Brief (94):1–8, PMID: 22617340.

Alexander M, Engel LS, Olaiya N, Wang L, Barrett J, Weems L, et al. 2018. The deepwater horizon oil spill coast guard cohort study: a cross-sectional study of acute respiratory health symptoms. Environ Res 162:196–202, PMID: 29331799, https://doi.org/10.1016/j.envres.2017.11.044.

Bartalesi B, Cavarra E, Fineschi S, Lucattelli M, Lunghi B, Martorana PA, et al. 2005. Different lung responses to cigarette smoke in two strains of mice sensitive to oxidants. Eur Respir J 25(1):15–22, PMID: 15640318, https://doi.org/10.1183/09031936.04.00067204.

Berse B, Brown LF, Van de Water L, Dvorak HF, Senger DR. 1992. Vascular permeability factor (vascular endothelial growth factor) gene is expressed differentially in normal tissues, macrophages, and tumors. Mol Biol Cell 3(2):211–220, PMID: 1550962, https://doi.org/10.1091/mbc.3.2.211.

Blacquière MJ, Hylkema MN, Postma DS, Geerlings M, Timens W, Melgert BN. 2010. Airway inflammation and remodeling in two mouse models of asthma: comparison of males and females. Int Arch Allergy Immunol 153(2):173–181, PMID: 20413985, https://doi.org/10.1159/000312635.

Campbell D, Cox D, Crum J, Foster K, Christie P, Brewster D. 1993. Initial effects of the grounding of the tanker Braer on health in Shetland. The Shetland Health Study Group. BMJ 307(6914):1251–1255, PMID: 8281057, https://doi.org/10.1136/bmj.307.6914.1251.

Campbell D, Cox D, Crum J, Foster K, Riley A. 1994. Later effects of grounding of tanker Braer on health in Shetland. BMJ 309(6957):773–774, PMID: 7950562, https://doi.org/10.1136/bmj.309.6957.773.

Carrasco JM, Lope V, Pérez-Gómez B, Aragonés N, Suárez B, López-Abente G, et al. 2006. Association between health information, use of protective devices and occurrence of acute health problems in the Prestige oil spill clean-up in Asturias and Cantabria (Spain): a cross-sectional study. BMC Public Health 6:1, PMID: 16390547, https://doi.org/10.1186/1471-2458-6-1.

Cheung D, Schot R, Zwinderman AH, Zagers H, Dijkman JH, Sterk PJ. 1997. Relationship between loss in parenchymal elastic recoil pressure and maximal airway narrowing in subjects with alpha1-antitrypsin deficiency. Am J Respir Crit Care Med 155(1):135–140, PMID: 9001302, https://doi.org/10.1164/ajrccm.155.1.9001302.

CSIC (Consejo Superior de Investigaciones Científicas). Ministry of Science and Education, Government of Spain. 2003. Informe Técnico CSIC "Prestige" No. 1. Caracterización del vertido y evolución preliminar en el medio (in Spanish). http://csicprestige.iim.csic.es/desarro/informcsic/1/index.htm [accessed 4 July 2019].

CSIC. Ministry of Science and Education, Government of Spain. 2005. Informe Técnico CSIC "Prestige" No. 10. Contenido de componentes volátiles en el fuel-oil vertido por el Prestige (in Spanish). http://csicprestige.iim.csic.es/desarro/informcsic/10/index.htm [accessed 4 July 2019].

Demedts IK, Demoor T, Bracke KR, Joos GF, Brusselle GG. 2006. Role of apoptosis in the pathogenesis of COPD and pulmonary emphysema. Respir Res 7:53, PMID: 16571143, https://doi.org/10.1186/1465-9921-7-53.

Dunnill MS. 1962. Quantitative methods in the study of pulmonary pathology. Thorax 17(4):320–328, PMID: 25269161, https://doi.org/10.1136/thx.17.4.320.

Eggleston PA. 2007. The environment and asthma in US inner cities. Chest 132(suppl 5):782S–788S, PMID: 17998342, https://doi.org/10.1378/chest.07-1906.

Gam KB, Engel LS, Kwok RK, Curry MD, Stewart PA, Stenzel MR, et al. 2018a. Association between Deepwater Horizon oil spill response and cleanup work experiences and lung function. Environ Int 121(Pt 1):695–702, PMID: 30317099, https://doi.org/10.1016/j.envint.2018.09.058.

Gam KB, Kwok RK, Engel LS, Curry MD, Stewart PA, Stenzel MR, et al. 2018b. Lung function in oil spill response workers 1-3 years after the Deepwater Horizon disaster. Epidemiology 29(3):315–322, PMID: 29381492, https://doi.org/10.1097/EDE.0000000000000808.

Goldstein BD, Osofsky HJ, Lichtveld MY. 2011. The Gulf oil spill. N Engl J Med 364(14):1334–1348, PMID: 21470011, https://doi.org/10.1056/NEJMra1007197.

Guerassimov A, Hoshino Y, Takubo Y, Turcotte A, Yamamoto M, Ghezzo H, et al. 2004. The development of emphysema in cigarette smoke-exposed mice is strain dependent. Am J Respir Crit Care Med 170(9):974–980, PMID: 15282203, https://doi.org/10.1164/rccm.200309-1270OC.

Hauser R, Elreedy S, Hoppin JA, Christiani DC. 1995. Airway obstruction in boilermakers exposed to fuel oil ash. A prospective investigation. Am J Respir Crit Care Med 152(5 Pt 1):1478–1484, PMID: 7582280, https://doi.org/10.1164/ajrccm.152.5.7582280.

Hsia CC, Hyde DM, Ochs M, Weibel ER, ATS/ERS Joint Task Force on Quantitative Assessment of Lung Structure. 2010. An official research policy statement of the American Thoracic Society/European Respiratory Society: standards for quantitative assessment of lung structure. Am J Respir Crit Care Med 181(4):394–418, PMID: 20130146, https://doi.org/10.1164/rccm.200809-1522ST.

Imai K, Mercer BA, Schulman LL, Sonett JR, D'Armiento JM. 2005. Correlation of lung surface area to apoptosis and proliferation in human emphysema. Eur Respir J 25(2):250–258, PMID: 15684288, https://doi.org/10.1183/09031936.05.00023704.

Janjua NZ, Kasi PM, Nawaz H, Farooqui SZ, Khuwaja UB, Najam ul H, et al. 2006. Acute health effects of the Tasman Spirit oil spill on residents of Karachi, Pakistan. BMC Public Health 6:84, PMID: 16584541, https://doi.org/10.1186/1471-2458-6-84.

Jernelöv A. 2010. The threats from oil spills: now, then, and in the future. Ambio 39(5–6):353–366, PMID: 21053719, https://doi.org/10.1007/s13280-010-0085-5.

Karol MH. 1983. Concentration-dependent immunologic response to toluene diisocyanate (TDI) following inhalation exposure. Toxicol Appl Pharmacol 68(2):229–241, PMID: 6304938, https://doi.org/10.1016/0041-008x(83)90007-8.

Kasahara Y, Tuder RM, Cool CD, Lynch DA, Flores SC, Voelkel NF. 2001. Endothelial cell death and decreased expression of vascular endothelial growth factor and vascular endothelial growth factor receptor 2 in emphysema. Am J Respir Crit Care Med 163(3 Pt 1):737–744, PMID: 11254533, https://doi.org/10.1164/ajrccm.163.3.2002117.

Kasahara Y, Tuder RM, Taraseviciene-Stewart L, Le Cras TD, Abman S, Hirth PK, et al. 2000. Inhibition of VEGF receptors causes lung cell apoptosis and emphysema. J Clin Invest 106(11):1311–1319, PMID: 11104784, https://doi.org/10.1172/JCI10259.

Kilkenny C, Browne WJ, Cuthill IC, Emerson M, Altman DG. 2010. Improving bioscience research reporting: the ARRIVE guidelines for reporting animal research. PLoS Biol 8(6):e1000412, PMID: 20613859, https://doi.org/10.1371/journal.pbio.1000412.

Koh DH, Chung EK, Jang JK, Lee HE, Ryu HW, Yoo KM, et al. 2014. Cancer incidence and mortality among temporary maintenance workers in a refinery/petrochemical complex in Korea. Int J Occup Environ Health 20(2):141–145, PMID: 24999849, https://doi.org/10.1179/2049396714Y.0000000059.

Koyama H, Nishimura K, Ikeda A, Sakai N, Mishima M, Izumi T. 1996. Influence of baseline airway calibre and pulmonary emphysema on bronchial responsiveness in patients with chronic obstructive pulmonary disease. Respir Med 90(6):323–328, PMID: 8759473, https://doi.org/10.1016/s0954-6111(96)90126-2.

Laffon B, Fraga-Iriso R, Pérez-Cadahía B, Méndez J. 2006. Genotoxicity associated to exposure to Prestige oil during autopsies and cleaning of oil-contaminated birds. Food Chem Toxicol 44(10):1714–1723, PMID: 16814914, https://doi.org/10.1016/j.fct.2006.05.010.

Leikauf GD. 2002. Hazardous air pollutants and asthma. Environ Health Perspect 110(suppl 4):505–526, PMID: 12194881, https://doi.org/10.1289/ehp.02110s4505.

Li X, Zhang Y, Liang Y, Cui Y, Yeung SC, Ip MS, et al. 2017. iPSC-derived mesenchymal stem cells exert SCF-dependent recovery of cigarette smoke-induced apoptosis/proliferation imbalance in airway cells. J Cell Mol Med 21(2):265–277, PMID: 27641240, https://doi.org/10.1111/jcmm.12962.

Lyons RA, Temple JM, Evans D, Fone DL, Palmer SR. 1999. Acute health effects of the Sea Empress oil spill. J Epidemiol Community Health 53(5):306–310, PMID: 10396538, https://doi.org/10.1136/jech.53.5.306.

Majo J, Ghezzo H, Cosio MG. 2001. Lymphocyte population and apoptosis in the lungs of smokers and their relation to emphysema. Eur Respir J 17(5):946–953, PMID: 11488331, https://doi.org/10.1183/09031936.01.17509460.

March TH, Wilder JA, Esparza DC, Cossey PY, Blair LF, Herrera LK, et al. 2006. Modulators of cigarette smoke-induced pulmonary emphysema in A/J mice. Toxicol Sci 92(2):545–559, PMID: 16699168, https://doi.org/10.1093/toxsci/kfl016.

Medford AR, Douglas SK, Godinho SI, Uppington KM, Armstrong L, Gillespie KM, et al. 2009. Vascular endothelial growth factor (VEGF) isoform expression and activity in human and murine lung injury. Respir Res 10:27, PMID: 19358726, https://doi.org/10.1186/1465-9921-10-27.

Meo SA, Al-Drees AM, Meo IM, Al-Saadi MM, Azeem MA. 2008. Lung function in subjects exposed to crude oil spill into sea water. Mar Pollut Bull 56(1):88–94, PMID: 18031764, https://doi.org/10.1016/j.marpolbul.2007.09.039.

Meo SA, Al-Drees AM, Rasheed S, Meo IM, Al-Saadi MM, Ghani HA, et al. 2009. Health complaints among subjects involved in oil cleanup operations during oil spillage from a Greek tanker "Tasman Spirit." Int J Occup Med Environ Health 22(2):143–148, PMID: 19546094, https://doi.org/10.2478/v10001-009-0011-x.

Mohamed Hoesein FA, Zanen P, de Jong PA, van Ginneken B, Boezen HM, Groen HJ, et al. 2013. Rate of progression of CT-quantified emphysema in male current and ex-smokers: a follow-up study. Respir Res 14:55, PMID: 23688060, https://doi.org/10.1186/1465-9921-14-55.

Moorman JE, Akinbami LJ, Bailey CM, Zahran HS, King ME, Johnson CA, et al. 2012. National surveillance of asthma: United States, 2001–2010. Vital Health Stat 3 (35):1–58, PMID: 24252609.

Morissette MC, Parent J, Milot J. 2009. Alveolar epithelial and endothelial cell apoptosis in emphysema: what we know and what we need to know. Int J Chron Obstruct Pulmon Dis 4:19–31, PMID: 19436685.

Morita A, Kusaka Y, Deguchi Y, Moriuchi A, Nakanaga Y, Iki M, et al. 1999. Acute health problems among the people engaged in the cleanup of the Nakhodka oil spill. Environ Res 81(3):185–194, PMID: 10585014, https://doi.org/10.1006/enrs.1999.3979.

Nurmatov U, Tagieva N, Semple S, Devereux G, Sheikh A. 2013. Volatile organic compounds and risk of asthma and allergy: a systematic review and meta-analysis of observational and interventional studies. Prim Care Respir J 22(1):PS9–PS15, PMID: 23460017, https://doi.org/10.4104/pcrj.2013.00010.

Parameswaran H, Majumdar A, Ito S, Alencar AM, Suki B. 2006. Quantitative characterization of airspace enlargement in emphysema. J Appl Physiol 100(1):186–193, PMID: 16166240, https://doi.org/10.1152/japplphysiol.00424.2005.

Pauluhn J. 2008. Comparative assessment of early acute lung injury in mice and rats exposed to 1,6-hexamethylene diisocyanate-polyisocyanate aerosols. Toxicology 247(1):33–45, PMID: 18375034, https://doi.org/10.1016/j.tox.2008.01.023.

Pusztaszeri MP, Seelentag W, Bosman FT. 2006. Immunohistochemical expression of endothelial markers CD31, CD34, von Willebrand factor, and Fli-1 in normal human tissues. J Histochem Cytochem 54(4):385–395, PMID: 16234507, https://doi.org/10.1369/jhc.4A6514.2005.

Raabe GK, Collingwood KW, Wong O. 1998. An updated mortality study of workers at a petroleum refinery in Beaumont, Texas. Am J Ind Med 33(1):61–81, PMID: 9408530, https://doi.org/10.1002/(SICI)1097-0274(199801)33:1<61::AID-AJIM8>3.0.CO;2-Z.

Ramos-Barbón D, Ludwig MS, Martin JG. 2004. Airway remodeling: lessons from animal models. Clin Rev Allergy Immunol 27(1):3–22, PMID: 15347847, https://doi.org/10.1385/CRIAI:27:1:003.

Ramos-Barbón D, Presley JF, Hamid QA, Fixman ED, Martin JG. 2005. Antigen-specific CD4+ T cells drive airway smooth muscle remodeling in experimental asthma. J Clin Invest 115(6):1580–1589, PMID: 15902312, https://doi.org/10.1172/JCI19711.

Robbesom AA, Versteeg EM, Veerkamp JH, van Krieken JH, Bulten HJ, Smits HT, et al. 2003. Morphological quantification of emphysema in small human lung specimens: comparison of methods and relation with clinical data. Mod Pathol 16(1):1–7, PMID: 12527706, https://doi.org/10.1097/01.MP.0000043519.29370.C2.

Rodríguez-Trigo G, Zock JP, Isidro Montes I. 2007. Health effects of exposure to oil spills (in Spanish). Arch Bronconeumol 43(11):628–635, PMID: 17983548, https://doi.org/10.1016/s1579-2129(07)60141-4.

Rodríguez-Trigo G, Zock JP, Pozo-Rodríguez F, Gómez FP, Monyarch G, Bouso L, et al. 2010. Health changes in fishermen 2 years after clean-up of the Prestige oil spill. Ann Intern Med 153(8):489–498, PMID: 20733177, https://doi.org/10.7326/0003-4819-153-8-201010190-00279.

Rodriguez-Trigo G, Zock JP, Verea H, Torralba Y, Bouso L, Gomez F, et al. 2006. Long-term effects on bronchial reactivity, oxidative stress and respiratory symptoms in fishermen who participated in clean-up activities of the Prestige oil spill. Eur Respir J 28(suppl 50):689.

Saetta M, Baraldo S, Corbino L, Turato G, Braccioni F, Rea F, et al. 1999. CD8+ve cells in the lungs of smokers with chronic obstructive pulmonary disease. Am J Respir Crit Care Med 160(2):711–717, PMID: 10430750, https://doi.org/10.1164/ajrccm.160.2.9812020.

Segura-Valdez L, Pardo A, Gaxiola M, Uhal BD, Becerril C, Selman M. 2000. Upregulation of gelatinases A and B, collagenases 1 and 2, and increased parenchymal cell death in COPD. Chest 117(3):684–694, PMID: 10712992, https://doi.org/10.1378/chest.117.3.684.

Singhal M, Khaliq F, Singhal S, Tandon OP. 2007. Pulmonary functions in petrol pump workers: a preliminary study. Indian J Physiol Pharmacol 51(3):244–248, PMID: 18341220.

Suárez B, Lope V, Pérez-Gómez B, Aragonés N, Rodríguez-Artalejo F, Marqués F, et al. 2005. Acute health problems among subjects involved in the cleanup operation following the Prestige oil spill in Asturias and Cantabria (Spain). Environ Res 99(3):413–424, PMID: 16307984, https://doi.org/10.1016/j.envres.2004.12.012.

Takeda M, Tanabe M, Ito W, Ueki S, Konnno Y, Chihara M, et al. 2013. Gender difference in allergic airway remodelling and immunoglobulin production in mouse model of asthma. Respirology 18(5):797–806, PMID: 23490273, https://doi.org/10.1111/resp.12078.

Tanabe N, Muro S, Sato S, Tanaka S, Oguma T, Kiyokawa H, et al. 2012. Longitudinal study of spatially heterogeneous emphysema progression in current smokers with chronic obstructive pulmonary disease. PLoS One 7(9):e44993, PMID: 23028728, https://doi.org/10.1371/journal.pone.0044993.

Tang K, Rossiter HB, Wagner PD, Breen EC. 2004. Lung-targeted VEGF inactivation leads to an emphysema phenotype in mice. J Appl Physiol 97(4):1559–1566, PMID: 15208295, https://doi.org/10.1152/japplphysiol.00221.2004.

Tokairin Y, Shibata Y, Sata M, Abe S, Takabatake N, Igarashi A, et al. 2008. Enhanced immediate inflammatory response to Streptococcus pneumoniae in the lungs of mice with pulmonary emphysema. Respirology 13(3):324–332, PMID: 18399852, https://doi.org/10.1111/j.1440-1843.2007.01229.x.

Tuder RM, Zhen L, Cho CY, Taraseviciene-Stewart L, Kasahara Y, Salvemini D, et al. 2003. Oxidative stress and apoptosis interact and cause emphysema due to vascular endothelial growth factor receptor blockade. Am J Respir Cell Mol Biol 29(1):88–97, PMID: 12600822, https://doi.org/10.1165/rcmb.2002-0228OC.

Uzma N, Salar BM, Kumar BS, Aziz N, David MA, Reddy VD. 2008. Impact of organic solvents and environmental pollutants on the physiological function in petrol filling workers. Int J Environ Res Public Health 5(3):139–146, PMID: 19139531, https://doi.org/10.3390/ijerph5030139.

Verhoeven GT, Verbraak AF, Boere-van der Straat S, Hoogsteden HC, Bogaard JM. 2000. Influence of lung parenchymal destruction on the different indexes of the methacholine dose-response curve in COPD patients. Chest 117(4):984–990, PMID: 10767228, https://doi.org/10.1378/chest.117.4.984.

Vincent MJ, Bernstein JA, Basketter D, LaKind JS, Dotson GS, Maier A. 2017. Chemical-induced asthma and the role of clinical, toxicological, exposure and epidemiological research in regulatory and hazard characterization approaches. Regul Toxicol Pharmacol 90:126–132, PMID: 28866265, https://doi.org/10.1016/j.yrtph.2017.08.018.

Woodin MA, Hauser R, Liu Y, Smith TJ, Siegel PD, Lewis DM, et al. 1998. Molecular markers of acute upper airway inflammation in workers exposed to fuel-oil ash. Am J Respir Crit Care Med 158(1):182–187, PMID: 9655727, https://doi.org/10.1164/ajrccm.158.1.9711054.

Wright JL, Sun JP. 1994. Effect of smoking cessation on pulmonary and cardiovascular function and structure: analysis of guinea pig model. J Appl Physiol 76(5):2163–2168, PMID: 8063682, https://doi.org/10.1152/jappl.1994.76.5.2163.

Yang SC, Lin BY. 2010. Comparison of airway hyperreactivity in chronic obstructive pulmonary disease and asthma. Chang Gung Med J 33(5):515–523, PMID: 20979702.

Zock JP, Rodríguez-Trigo G, Pozo-Rodríguez F, Barberà JA. 2011. Health effects of oil spills: lessons from the Prestige. Am J Respir Crit Care Med 184(10):1094–1096, PMID: 21719754, https://doi.org/10.1164/rccm.201102-0328ED.

Zock JP, Rodríguez-Trigo G, Pozo-Rodríguez F, Barberà JA, Bouso L, Torralba Y, et al. 2007. Prolonged respiratory symptoms in clean-up workers of the Prestige oil spill. Am J Respir Crit Care Med 176(6):610–616, PMID: 17556713, https://doi.org/10.1164/rccm.200701-016OC.

Zock JP, Rodríguez-Trigo G, Rodríguez-Rodríguez E, Espinosa A, Pozo-Rodríguez F, Gómez F, et al. 2012. Persistent respiratory symptoms in clean-up workers 5 years after the Prestige oil spill. Occup Environ Med 69(7):508–513, PMID: 22539655, https://doi.org/10.1136/oemed-2011-100614.